Optica Applicata, Vol. XXVII, No. 3, 1997

Theoretical analysis of SE and BSE signals applied to SEM multiple detector systems

D. KACZMAREK

Institute of Electronic Technology, Technical University of Wrocław, ul. Janiszewskiego 11/17, 50–372 Wrocław, Poland.

In this paper, a theoretical analysis concerning the secondary electron (SE) signal and backscattered electron (BSE) signal in scanning electron microscope has been presented. A simplified model of angular dependence of electron beam–solid interactions has been assumed. Results of the work concern the samples with weak material and topographic contrasts. It has been shown that for this case and small angles of incidence of the primary beam in SEM the current densities of SE and BSE can be represented by a series. The terms of the series containing the information on topography (TOPO) and composition (COMPO) only, as well as the terms of disturbance character, have been separated. On the basis of theoretical analysis a method of TOPO and COMPO signals separation has been proposed which consists in introduction of the appropriate correction. The algorithm of obtaining both TOPO and COMPO signals in SEM by analogous and digital methods have been described. The SEM images obtained by different algorithms have been compared.

1. Introduction

Signals of secondary electrons (SE) and backscattered electrons (BSE) are widely used for examination of surfaces in scanning electron microscopes (SEM) [1]–[6]. For detection of these signals both standard configuration of detectors as well as multidetector sets are employed [4], [7]–[9]. Numerous papers are devoted to improvement of detection methods in order to gain better separation of topographic (TOPO) and composition (COMPO) modes [1], [10]–[12]. So, the different methods of mixing signals coming from various SEM detectors [9], [10] as well as the proposed optimum layout of detectors in respect of the specimen location [13], [14] have been presented. The problem is very important and still the solutions obtained both by experimental [1], [6], [9] and theoretical methods [3], [15]–[18] are being searched. The current article is just a contribution to such searches.

2. Geometrical theory in the case of secondary and backscattered electrons

The primary electron beam in a scanning electron microscope incident on a specimen surface releases electrons, photons and ions with widespread energetic spectra. In the scanning microscopy important information about the specimen is contained in the emission of backscattered electrons [19].

The secondary electrons can be divided into electrons with energy lower than 50 eV, so-called real secondary electrons (SE), and electrons with energy higher than 50 eV, so-called backscattered electrons (BSE) [20]. Both kinds of the electrons carry the information about the interfaces located at different depths under the specimen surface and are featured with various angular distributions (Fig. 1).

Fig. 1. Angular characteristics: **a** — SE, **b** — BSE. (I_0 — primary beam, N — normal to the specimen surface)

The secondary electrons at the slant incidence of primary beam I_0 are featured with the angular distribution symmetrical in relation to the normal N (Fig. 1**a**), whereas the angular characteristic of backscattered electrons (Fig. 1**b**) is asymmetrical and has one privileged direction corresponding to reflected electrons. The theory concerning BSE signals has been presented, however, since the analysis of such kind of signals is difficult because of the complex relationship describing angular density of BSE, the formulae for SE have been derived first in order to show the basic assumptions of the method of calculations.

2.1. Angular characteristics of backscattered electrons with the shape factor *n* being taken into account

Angular density of the current of backscattered electrons can be written as [4]

$$j = \frac{dI}{d\Omega} = A\cos^{-n}\alpha\cos\theta \tag{1}$$

where: I — total current of backscattered electrons, Ω — solid angle, θ — angle of detection (the point-dimensions of detector have been assumed), α — angle of primary electron beam incidence contained between the incident beam and the normal to the surface, carrying the information about surface topograpgh (Fig. 2a), A — material constant equal to $1/\pi\delta_{(0)}$ (where $\delta_{(0)}$ is a brightness factor, representing particular material); as it results from experiment [4], $\delta_{(0)}$ is the monotonic function of the atomic number Z; n— experimental factor on which cosine distribution depends; if $n > 1$, the characteristics are expanded along y axis, if $n < 1$, the characteristics are flattened. Exponent n decreases monotonically with the increase in atomic number Z (Tab. 1).

The relationship (1) can be written as

$$j = \frac{1}{\pi}\delta_{(0)}\frac{\cos\theta}{\cos^n\alpha}, \tag{2}$$

i.e., for θ, $\alpha = \text{const}$, $j = f(\delta_{(0)}, n)$. (3)

Table 1. Dependence of exponent n on the atomic number Z [21]

	Z	n
Be	4	1.3
Al	13	1.1
Cu	29	0.89
Ag	47	0.72
Au	79	0.65

Both kinds of material contrast components can be differentiated with respect to $\delta_{(0)}$ and n:

$$\frac{\partial j}{\partial(\delta_{(0)})} = \frac{1}{\pi}\frac{\cos 0}{\cos^n \alpha}, \tag{4}$$

$$\frac{\partial j}{\partial n} = -\frac{1}{\pi}\frac{\cos 0 \ln\cos\alpha}{\cos^n \alpha}. \tag{5}$$

Dividing relationships (4) and (5), we can get the ratio of both contrast components

$$C = \frac{\partial j/\partial n}{\partial j/\partial(\delta_{(0)})} = -\ln\cos\alpha. \tag{6}$$

The relationship between coefficient C and angle α is shown in Table 2.

Table 2. The dependence of coefficient C on the angle α [21]

α	C
0	0
30	0.1438
45	0.3466
60	0.6931
70	1.0729
80	1.7507
85	2.4401
90	infinity

The ratio of material contrast component dependent on n and the contrast component dependent on $\delta_{(0)}$ is equal to 0 for $\alpha = 0°$ and it increases slowly with the increase of angle α. Faster growth of the ratio takes place scarcely for angles α close to 90°, when C tends to infinity. It is difficult for angles α to approach close to 90°, because of the limited design abilities of the work chamber of SEM.

2.2. Theory of small signals referred to secondary electrons

In the following section, the case of secondary electrons (SE) more convenient for analysis because of the symmetry of angular characteristic will be taken into

consideration (Fig. 1a). The relationship between angles α, θ, θ_0, φ, describing mutual layout in the arrangement: beam – specimen – detector (Fig. 2), follows from Albatani theorem – the basic theorem in spherical geometry [4], [19]

$$\cos\theta = \cos\theta_0 \cos\alpha + \cos\theta_0 \sin\alpha \cos\varphi. \tag{7}$$

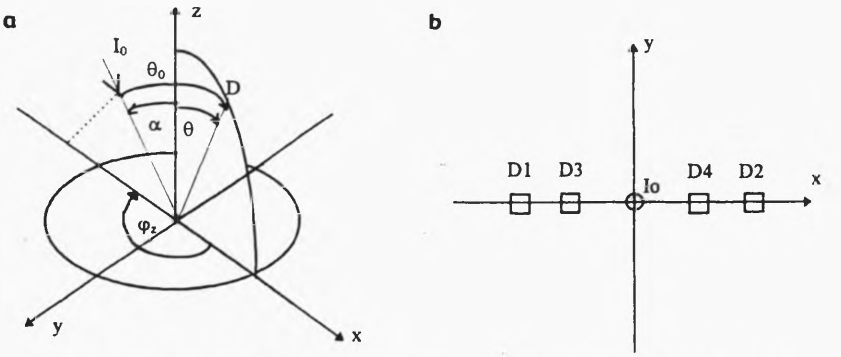

Fig. 2. Demonstration of: **a** – angles considered in geometrical theory, **b** – layout of detectors (I_0 – primary beam, D1 – D4 – detectors, α – angle of primary beam incidence, θ – detection angle, θ_0 – angle between the primary beam and detector, φ – azimuth angle)

Assuming $n = 1$ (when SE distribution is cosine), the angular density of secondary electrons, based on Eq. (1), can be expressed as

$$j = j(A,\alpha) = A(\cos\theta_0 + \sin\theta_0 \operatorname{tg}\alpha \cos\varphi), \tag{8}$$

where: A – information carrier about the kind of material, α – information carrier about surface topography.

According to the assumptions of small-signal theory, φ_z angle is approximately equal to azimuth angle measured in the plane perpendicular to primary beam $\varphi_I = \varphi$. The assumption is valid especially for higher detection angles θ_0 as well as in the case of $\varphi \approx 0$ and $\varphi \approx \Pi$.

According to the small signal theory (4) we can assume that α (Fig. 2) is low. We can calculate the partial derivatives of Eq. (8) and then expand them into Taylor's series for the function of two variables:

$$j(A,\alpha) = j_A dA + j_\alpha d\alpha + \frac{1}{2!}[j_{AA}(dA)^2 + 2j_{A\alpha} dA d\alpha + j_{\alpha\alpha}(d\alpha)^2], \tag{9}$$

$$j_A = \cos\theta_0 + \sin\theta_0 \operatorname{tg}\alpha \cos\varphi \approx \cos\theta_0, \tag{10}$$

$$j_{AA} = 0, \tag{11}$$

$$j_{A\alpha} = \cos\theta_0 + \frac{\sin\theta_0 \cos\varphi}{\cos^2\alpha} \approx \cos\theta_0 + \sin\theta_0 \cos\varphi, \tag{12}$$

$$j_\alpha = A \sin\theta_0 \frac{\cos\varphi}{\cos^2\alpha} \approx A \sin\theta_0 \cos\varphi, \tag{13}$$

$$j_{\alpha\alpha} = A\frac{\sin\theta_0\, 2\sin\alpha\cos\varphi}{\cos^4\alpha} \approx 0. \tag{14}$$

Substituting relationships (10)–(14) into Eq. (9) we can get:

$$j(A,\alpha) = j(A_0,0)+(\cos\theta_0 dA + A\sin\theta_0\cos\varphi d\alpha)$$

$$+\frac{1}{2!}[2(\cos\theta_0+\sin\theta_0\cos\varphi)dAd\alpha]. \tag{15}$$

In Equation (15), the first term $\cos\theta_0\, dA$ carries the information about material contained in the factor dA. It is called COMPO signal, whereas the second term $A\sin\theta_0\cos\varphi\, d\alpha$ describes topography and is called TOPO signal. For the theory of small signals, connected with the changes in material composition and topography, we can get

$$j = \cos\theta_0\, dA + A\sin\theta_0\cos\varphi\, d\alpha. \tag{16}$$

The following terms in (9) have the disturbance character and in the case of $dAd\alpha$ can be considered as TOPO·COMPO and for α^2 as TOPO^2. To separate signals of COMPO mode, the signals from two opposed detectors D3, D4 (Fig. 2), located at the angles $\varphi = 0(dj_0)$ and $\varphi = \pi(dj_\pi)$ [4], should be added. In such a case the total signal from the two detectors is according to (15)

$$dj = dj_0 + dj_\pi = 2\cos\theta_0 dA. \tag{17}$$

As can be seen, the signal is especially strong at the zenith at arrangement of the detectors ($\theta_0 = 0$). By subtracting the signals from two opposed detectors D1, D2 (Fig. 2b), based on relationship (15), we can get TOPO signal

$$dj = dj_0 - dj_\pi = 2A\sin\theta_0\cos\varphi d\alpha. \tag{18}$$

The signal is especially strong at the possible horizontal arrangement of the detectors ($\theta_0 = \pi/2$), with $\cos\varphi$ different from 0. Generalizing, it can be stated that the dependences similar to (17) and (18) are valid for each detector pair placed symmetrically to the primary beam.

The above consideration concerning secondary electrons can be a basis for carrying out the analysis for more complex arrangements electron beam–specimen–detector. In the following section, the analysis of backscattered electrons will be performed, taking into account all problems emerging in effect of non-cosine distribution of BSE (Fig. 1b).

2.3. Small signal theory with respect to backscattered electrons

Analogous consideration as for secondary electrons is in the case of backscattered electrons much more complex because of the difficulty in obtaining the appropriate relationship for the angular density BSE current, like equation (1). However, determination of angular characteristics of backscattered electrons can be done using simplified models. According to MURATA [22], who compiled Rutherford's law of

scattering [17] with Everhart's model of single-scattering [20] and Thomson –Whiddington's law of energetic losses [20], the angular density $dI/d\Omega$ can be expressed as

$$j = \frac{dI}{d\Omega} = A\cos^2\alpha\left[1-\left(\frac{\cos\alpha}{\cos\theta+\cos\alpha}\right)^{a/\cos^2\alpha}\right](1+\cos\theta\cos\alpha+\sin\theta\sin\alpha\cos\varphi)^2. \quad (19)$$

From (19) it follows that the angular density $dI/d\Omega$ strongly depends on the azimuth angle φ. More comprehensive analysis of backscattered electrons introduces additional disturbance terms into relationships (17) and (18). This follows from the fact that, assuming $\alpha = 0$ in dependences (9), (12) and (13), we have neglected the small signal terms $\mathrm{tg}\alpha$, $1/\cos^2\alpha$ and $2\sin\alpha/\cos^4\alpha$. If we take them into account, we will get an additional disturbance term, proportional to α^2 in Eq. (17), describing COMPO signal and an additional disturbance term, proportional to $dA\alpha$ in Eq. (18), describing TOPO signal. So, we have:

$$dj = 2\cos\theta_0 dA + f_3\alpha^2, \quad (20)$$

$$dj = 2A\sin\theta_0\cos\varphi\, d\alpha + f_4\alpha dA. \quad (21)$$

Introducing (20) and (21) into relationship (16) we get the expression

$$dj = 2\cos\theta_0 dA + 2A\sin\theta_0\cos\varphi\, d\alpha + f_3\alpha^2 + f_4\alpha dA. \quad (22)$$

In the following section, the influence of higher harmonic terms on BSE signals, which were used for simulation of signals coming from the specimen to the detectors, will be considered.

2.4. Regarding higher harmonic terms in the theory of small-signals with respect to BSE

For example, a case where the primary beam and the normal to the specimen surface as well as the detection line are located on the same plane ($\varphi = 0, \Pi$) will be considered. Equation (7) can be then expressed as $\theta = \theta_0 \pm \alpha$. This relationship has been introduced to Eq. (19) and relationship (23) has been obtained. Next, the relationship has been expanded into a series of α:

$$j = A\cos^2\alpha\left[1-\left(\frac{\cos\alpha}{\cos(\theta_0+\alpha)+\cos\alpha}\right)^{a/\cos^2\alpha}\right]$$
$$\times[1+\cos(\theta_0+\alpha)\cos\alpha+\sin(\theta_0+\alpha)\sin\alpha\cos\varphi]^2. \quad (23)$$

Introducing small signal theory, we can assume that:

$$\alpha \approx 0 \to \cos\alpha \approx 1-\frac{\alpha^2}{2}, \quad \cos^2\alpha \approx 1-\sin^2\alpha = 1-\alpha^2, \quad \sin\alpha \approx \alpha, \quad (24)$$

$$\varphi = 0 \to \cos\varphi = 1, \quad (25)$$

$$\cos(\theta_0+\alpha)\cos\alpha+\sin(\theta_0+\alpha)\sin\alpha = \cos(\theta_0+\alpha-\alpha) = \cos\theta_0, \quad (26)$$

$$\frac{1}{[1+\cos(\theta_0+\alpha)\cos\alpha+\sin(\theta_0+\alpha)\sin\alpha]^2}=\frac{1}{(1+\cos\theta_0)^2}, \tag{27}$$

$$\cos(\theta_0+\alpha)=\cos\theta_0-(\sin\theta_0)\alpha-\frac{\cos\theta_0}{2}\alpha^2=\cos\theta_0\left[1-(\mathrm{tg}\,\theta_0)\alpha-\frac{1}{2}\alpha^2\right], \tag{28}$$

$$\frac{\cos\alpha}{\cos(\theta_0+\alpha)+\cos\alpha}=\frac{1-\frac{\alpha^2}{2}}{\cos\theta_0-(\sin\theta_0)\alpha-\frac{\cos\theta_0}{2}\alpha^2+\left(1-\frac{\alpha^2}{2}\right)}, \tag{29}$$

$$\frac{\cos\alpha}{\cos(\theta_0+\alpha)+\cos\alpha}=\frac{1-\frac{\alpha^2}{2}}{(1+\cos\theta_0)-(\sin\theta_0)\alpha-(1+\cos\theta_0)\frac{\alpha^2}{2}}, \tag{30}$$

$$f^{\frac{a}{\cos^2\alpha}}\simeq f^{\frac{a}{1-\alpha^2}}\simeq f^{a(1+\alpha^2)}, \tag{31}$$

$$f^{\frac{a}{\cos^2\alpha}}\simeq e^{a(1+\alpha^2)\ln f}, \tag{32}$$

$$f^{\frac{a}{\cos^2\alpha}}\simeq e^{a\ln f}e^{a\ln f\alpha^2}, \tag{33}$$

$$f^{\frac{a}{\cos^2\alpha}}=e^{a\ln f}(1+a\ln f\alpha^2)=f^a(1+a\ln f\alpha^2), \tag{34}$$

$$f=\frac{1}{1+\cos\theta_0}, \tag{35}$$

$$f^{\frac{a}{\cos^2\alpha}}=\frac{1}{(1+\cos\theta_0)^a}\left[1+\left(a\ln\frac{1}{1+\cos\theta_0}\right)\alpha^2\right] \tag{36}$$

After regarding relationships (26)–(36), the angular density of BSE can be expressed as:

$$j=A_0\left(1+\frac{dA}{A_0}\right)\left(1-\frac{\alpha^2}{2}\right)\times\left\{1-\frac{1}{(1+\cos\theta_0)^a}\left(1+\frac{a}{2}\ln\frac{1}{1+\cos\theta_0}\alpha^2\right)\right.$$
$$\left.\times\left(1+a\frac{\sin\theta_0}{1+\cos\theta_0}\alpha+\frac{a}{2}\frac{\sin^2\theta_0}{(1+\cos\theta_0)^2}\alpha^2\right)\right\}\times\frac{1}{(1+\cos\theta_0)^2}, \tag{37}$$

$$j=A_0(1+\cos\theta_0)^2\left(1+\frac{dA}{A_0}\right)\left(1-\frac{\alpha^2}{2}\right)\Bigg]$$
$$\times\left\{1-\frac{1}{(1+\cos\theta_0)^a}\left[1+a\frac{\sin\theta_0}{1+\cos\theta_0}\alpha+\left(\frac{a}{2}\ln\frac{1}{1+\cos\theta_0}+\frac{a}{2}\frac{\sin^2\theta_0}{(1+\cos\theta_0)^2}\alpha^2\right)\right]\right\}, \tag{38}$$

$$j = A_0(1+\cos\theta_0)^2\left(1+\frac{dA}{A_0}\right)\left(1-\frac{\alpha^2}{2}\right)\times\left\{\left(1-\frac{1}{(1+\cos\theta_0)^a}\right)-\frac{1}{(1+\cos\theta_0)^a}\right.$$
$$\left.\times\left[a\frac{\sin\theta_0}{1+\cos\theta_0}\alpha+\left(\frac{a}{2}\ln\frac{1}{1+\cos\theta_0}+\frac{a}{2}\frac{\sin^2\theta_0}{(1+\cos\theta_0)^2}\right)\alpha^2\right]\right\}, \tag{39}$$

$$j = A_0(1+\cos\theta_0)^2\left[1-\frac{1}{(1+\cos\theta_0)^a}\right]\left(1+\frac{dA}{A_0}\right)\left(1-\frac{\alpha^2}{2}\right)$$
$$\times\left\{1-\frac{1}{(1+\cos\theta_0)^a-1}\left[a\frac{\sin\theta_0}{1+\cos\theta_0}\alpha+\left(\frac{a}{2}\ln\frac{1}{1+\cos\theta_0}+\frac{a}{2}\frac{\sin^2\theta_0}{(1+\cos\theta_0)^2}\right)\alpha^2\right]\right\}. \tag{40}$$

A natural generalization of Eq. (40) can be described as follows:

$$dj = f_0(1+f_1 dA+f_2\alpha+f_3\alpha^2+f_4 dA\alpha), \tag{41}$$

$$f_0 = A_0(1+\cos\theta_0)^2\left[1-\frac{1}{(1+\cos\theta_0)^a}\right]d\Omega, \tag{42}$$

$$f_1 = \frac{1}{A_0}, \tag{43}$$

$$f_2 = -\frac{1}{(1+\cos\theta_0)^a-1}\frac{a\sin\theta_0}{1+\cos\theta_0}, \tag{44}$$

$$f_3 = \frac{-1}{(1+\cos\theta_0)^a-1}\frac{a}{2}\left[\ln\frac{1}{1+\cos\theta_0}+\frac{\sin^2\theta_0}{(1+\cos\theta_0)^2}\right]-\frac{1}{2}, \tag{45}$$

$$f_4 = \frac{1}{A_0}f_2, \tag{46}$$

where: θ_0 – detection angle (Fig. 2), $d\Omega$ – solid angle of detector, α – angle of primary beam incidence with respect to the normal, A_0, a – constants proportional to atomic number Z, with $A_0 = a$ [23].

For example, NIEDRIG [20] designates constant a as equal to $0.045Z$. The author assumes that $a = 0.037Z$ (after [17]).

The term with factor f_1 corresponds to COMPO signal, whereas the one with factor f_2 corresponds to TOPO signal. The following terms have disturbance character and are TOPO^2 and TOPO·COMPO, respectively.

3. Practical realization of the theory results

From the geometric theory it follows that summing up BSE signals from single detectors causes disappearance of all terms with α and odd powers in Eq. (41). The term TOPO^2 remains, however, as a disturbance in the COMPO mode thus created.

Subtraction of BSE signals from single detectors causes, on the other hand, disappearance of all terms with α and even powers in Eq. (41). The expression TOPO·COMPO remains as a disturbance in the TOPO mode thus created.

Based on the presented theoretical analysis, a compensation of these disturbing signals has been proposed. According to this assumption, the creation of corrected COMPO mode ($COMPO_{COR}$) as well as corrected TOPO mode ($TOPO_{COR}$) should follow the algorithm:

$$COMPO_{COR} = (D3+D4)-\beta(D1-D2)^2, \tag{47}$$

$$TOPO_{COR} = (D1-D2)-\gamma(D1-D2)(D3+D4) \tag{48}$$

where: D1, D2, D3, D4 are BSE signals from detectors arranged as in Fig. 2**b**, β is the correction coefficient of COMPO mode chosen experimentally ($\beta \approx -0.05$), γ is the correction coefficient of TOPO mode chosen experimentally ($\gamma \approx +0.03$).

In Figure 3, digital images of SEM obtained on the basis of relationships following from the geometric theory are presented. In this figure, Ta surface scratched with the use of iron blade has been shown.

In Figures 3**a** and 3**b**, images of specimen topography obtained in a traditional way and after employing the correction of TOPO mode are compared. The configuration of surface (especially at location of scratches) is better distinguishable in Fig. 3**b**. As follows from relationship (48), signals from four detectors (D1, D2, D3 and D4 from Fig. 2**b**) were necessary for reconstruction of surface topography.

In effect of experimental investigations it has been stated that it is possible to employ only two detectors: D3 and D4 (Fig. 2**b**). This can be seen in Fig. 3**c**, where the image is created according to the algorithm

$$TOPO_{OPT} = (D3-D4)-\gamma(D3-D4)(D3+D4). \tag{49}$$

The arrow in Figure 3**c** shows that steep edges of the scratch are reconstructed better than in Fig. 3**b**.

Next, in Figures 3**d**,**e**,**f** digital images of composition of the same specimen are presented. As follows from Fig. 3**f**, in the case of COMPO mode, the algorithm based on signals from only two detectors (D3 and D4 in Fig. 2**b**) can be successfully employed instead of the algorithm described with Eq. (47)

$$COMPO_{OPT} = (D3+D4)-\beta(D3-D4)^2. \tag{50}$$

The material analysis with the use of digital method of colour simulation has shown that in the place of the scratches there are black areas of the rust from iron blade.

The conclusion can be drawn that proper reconstruction of surface for one direction of detection can be obtained based on BSE signals from two detectors arranged close to each other.

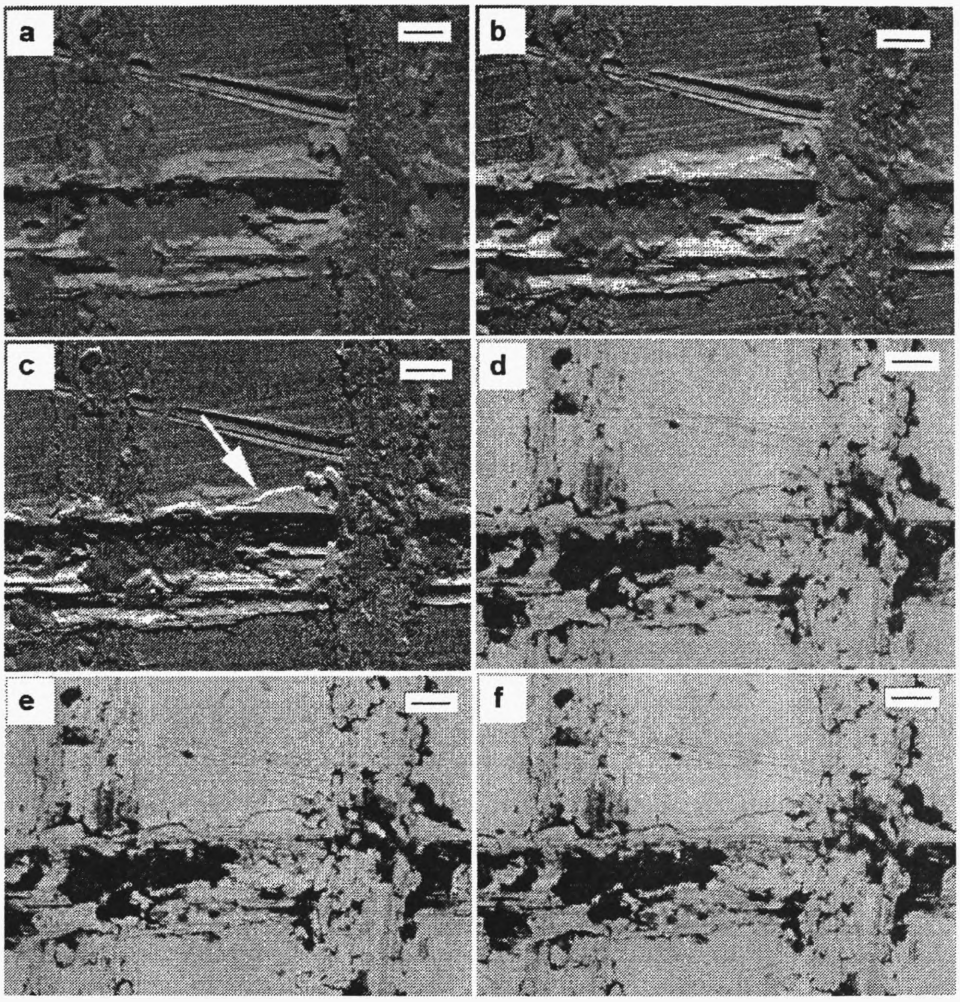

Fig. 3. Digital images of scratched Ta surface obtained in the modes: **a** – TOPO (D1−D2), **b** – $TOPO_{COR}$, according to relationship (48), **c** – $TOPO_{OPT}$, **d** – COMPO (D3+D4), **e** – $COMPO_{COR}$, according to relationship (47), **f** – $COMPO_{OPT}$. Bar = 25 μm

4. Summary

The paper presents a theoretical model for description of backscattered electron signal in SEM. The methods which can be used for correct reconstruction of surface topography and composition have been proposed. The results indicate that the real image of a specimen can be obtained on the basis of signals from two detectors (for each direction of detection x and y separately). The best fitting coefficients of correction terms have been chosen and it has been evidenced that the proposed theoretical model enables better separation of TOPO and COMPO modes in SEM.

Acknowledgements — Special thanks are due to Prof. Andrzej Mulak, Wrocław University of Technology, for invaluable help and stimulating discussion.

References

[1] BEIL W., CARLSEN I., J. Microscopy **157** (1990), 127.
[2] KACZMAREK D., Beitr. Elektronenmikroskop. Direktabb. Oberfl. **22** (1989), 129.
[3] RADZIMSKI Z., J. Computer-Assisted Microscopy **6** (1994), 149.
[4] REIMER L., BÖNGELER R., DESAI V., Scanning Microscopy **1** (1987), 963.
[5] SCHOU J., Scanning Microscopy **3** (1989), 429.
[6] SUGANUMA T., J. Electron Microscopy **34** (1985), 328.
[7] MULAK A., KACZMAREK D., Beitr. Electronenmikroskop. Direktabb. Oberfl. **23** (1990), 357.
[8] NIEMIETZ A., REIMER L., Ultramicroscopy **16** (1985), 161.
[9] REIMER L., RIEPENHAUSEN M., Scanning **7** (1985), 221.
[10] KACZMAREK D., KORDAS L., CZYŻEWSKI Z., DĄBROWSKA-SZATA M., MULAK A., ROMANOWSKI A., WIKIERA R., Opt. Appl. **19** (1989), 301.
[11] KOTERA M., FUJIWARA T., SUGA H., Jpn. J. Appl. Phys. **29** (1990), 2312.
[12] KACZMAREK D., KORDAS L., Beitr. Elektronenmikroskop. Direktabb. Oberfl. **25** (1992), 103.
[13] KACZMAREK D., ANDRZEJEWSKI P., Proc. SPIE **2780** (1995), 125.
[14] HEJNA J., Scanning Microscopy **8** (1994), 143.
[15] DESAI V., REIMER L., Scanning **12** (1990), 1.
[16] KOTERA M., FUJIWARA T., SUGA H., WITTRY D., Jpn. J. Appl. Phys. **29** (1990), 2317.
[17] MURATA K., J. Appl. Phys. **45** (1974), 4110.
[18] WINKLER H., GROSS H., Scanning Microscopy, Suppl., **2** (1988), 379.
[19] JOY D., J. Microscopy **136** (1984), 241.
[20] NIEDRIG H., SEM Inc. **1** (1984), 51.
[21] MULAK A., KACZMAREK D., Proc. Intern. Conf. on Electron Beam Technologies, Varna 1991, p. 631.
[22] MURATA K., Phys. Status Solidi A **36** (1976), 197.
[23] MULAK A., KACZMAREK D., Proc. the XIIth Intern. Congress for Electron Microscopy, San Francisco, 1990, p. 412.

Received May 14, 1997
in revised form September 3, 1997